Spatial pair correlations of atoms in molecular dissociation

C. M. Savage[1] and K. V. Kheruntsyan[2]

[1]*ARC Centre of Excellence for Quantum-Atom Optics, Department of Physics, Australian National University, Canberra ACT 0200, Australia*

[2]*ARC Centre of Excellence for Quantum-Atom Optics, School of Physical Sciences, University of Queensland, Brisbane, QLD 4072, Australia*

(Dated: February 1, 2008)

We perform first-principles quantum simulations of dissociation of trapped, spatially inhomogeneous Bose-Einstein condensates of molecular dimers. Specifically, we study spatial pair correlations of atoms produced in dissociation after time of flight. We find that the observable correlations may significantly degrade in systems with spatial inhomogeneity compared to the predictions of idealized uniform models. We show how binning of the signal can enhance the detectable correlations and lead to the violation of the classical Cauchy-Schwartz inequality and relative number squeezing.

PACS numbers: 03.75.Nt, 03.65.Ud, 03.75.Gg

Producing and utilizing quantum mechanical correlations between entangled particle pairs are major themes in quantum mechanics research. In this paper we investigate correlations of the kind used by Einstein, Podolsky and Rosen (EPR) to argue that local realism is inconsistent with quantum mechanics being a complete theory of nature [1]. EPR type non-local correlations were first produced experimentally in the form of photon pairs from nondegenerate parametric down-conversion [2]. Here, the correlations are observed between the optical quadrature amplitudes of spatially separated signal and idler beams, which are analogous to canonical position and momentum variables originally discussed by EPR.

It should be possible to extend this type of experiment to ultra-cold atoms, which would allow the investigation of EPR correlations for particles with non-zero rest mass. These might be produced by the transfer of correlations from photons to atoms [3], or else by nonlinear matter-wave interactions. The latter include atomic four-wave mixing via Bose-Einstein condensate (BEC) collisions [4, 5] and matter-wave down-conversion via dissociation of a molecular BEC [6, 7, 8, 9]. Although the direct measurement of matter-wave quadrature correlations of this type is a challenging task [9], a simpler measurement of density-density correlations – as a prerequisite for the EPR quadrature correlations – can be performed with current experimental techniques.

In this paper we perform first-principles quantum simulations of dissociation of a BEC of molecular dimers into pair-correlated bosonic atoms. This has been demonstrated experimentally using ultracold (but not Bose condensed) $^{87}Rb_2$ dimers [10], although the atom correlations have not yet been measured. In the case of fermionic atoms [11, 12], such as in dissociation of $^{40}K_2$ dimers [13], the density-density correlations between the atoms in two different spin states have been measured; this case, however, currently resists first-principles quantum simulations. Nevertheless, many insights from the present bosonic case also apply to the fermionic case, and to correlations produced via BEC four-wave mixing [14]. For example; the importance of operationally well defined measures of correlations, the role of spatial inhomogeneity, and the trade-off between image resolution and binning to enhance correlation detection.

Measurements now challenge theory to give precise quantitative descriptions of the observable correlations. Experiments measuring atom shot noise in absorption images [13, 15, 16] and using microchannel plate detectors [17] have demonstrated atom-atom correlations [13, 14]. However, their quantitative theoretical analysis is lacking. There is also a need to determine the best operational measures [12, 18] of correlations for these experiments. The present work is a step towards these goals, and a benchmark for other (approximate) theories.

Previous theoretical work on molecular dissociation has explored the atomic correlations in simplified cases such as 1D systems [7, 9], without depletion of the molecules during conversion [12], or for spatially uniform systems [11, 18]. The present work builds on the characterization of the atomic correlations in momentum space in Ref. [18]. Here, we extend the analysis to spatial correlations and study molecular dissociation in 3D under experimentally realistic conditions, including the effects of inhomogeneity of the initial molecular BEC [19] and time-of-flight expansion. We focus on the use of absorption images, obtained by line of sight integration, to measure the atomic correlations.

To investigate the quantum dynamics of molecular dissociation we use stochastic equations in the positive P-representation [20]. In this method, one simulates the evolution of four complex stochastic (c-number) fields $\Psi_i(\mathbf{x},t)$ and $\Phi_i(\mathbf{x},t)$ $[\Phi_i^*(\mathbf{x},t) \neq \Psi_i(\mathbf{x},t)]$, representing the field operators $\hat{\Psi}_i(\mathbf{x},t)$ and $\hat{\Psi}_i^\dagger(\mathbf{x},t)$, respectively, where $i=0$ stands for molecules and $i=1$ for atoms. Averages of the stochastic field products over a large number of trajectories $\langle\ldots\rangle_{\rm st}$ correspond to quantum mechanical ensemble averages of normally-ordered operator moments. For example $\langle[\hat{\Psi}_i^\dagger(\mathbf{x},t)]^k[\hat{\Psi}_j(\mathbf{x}',t)]^n\rangle =$

$\langle[\Phi_i(\mathbf{x},t)]^k[\Psi_j(\mathbf{x}',t)]^n\rangle_{\rm st}$.

The stochastic differential equations governing the quantum dynamics of dissociation are [18]

$$\begin{aligned}
\frac{\partial\Psi_1}{\partial t} &= \frac{i\hbar}{2m_1}\nabla^2\Psi_1 - i\,\Delta\Psi_1 + \chi\Psi_0\Phi_1 + \sqrt{\chi\Psi_0}\,\zeta_1,\\
\frac{\partial\Phi_1}{\partial t} &= -\frac{i\hbar}{2m_1}\nabla^2\Phi_1 + i\Delta\Phi_1 + \chi\Phi_0\Psi_1 + \sqrt{\chi\Phi_0}\,\zeta_2,\\
\frac{\partial\Psi_0}{\partial t} &= \frac{i\hbar}{2m_0}\nabla^2\Psi_0 - \frac{\chi}{2}\Psi_1^2,\\
\frac{\partial\Phi_0}{\partial t} &= -\frac{i\hbar}{2m_0}\nabla^2\Phi_0 - \frac{\chi}{2}\Phi_1^2.
\end{aligned} \tag{1}$$

Here, $\zeta_j(\mathbf{x},t)$ ($j=1,2$) are real, independent Gaussian noises with zero means and nonzero correlations $\langle\zeta_j(\mathbf{x},t)\zeta_k(\mathbf{x}',t')\rangle_{\rm st} = \delta_{jk}\delta(\mathbf{x}-\mathbf{x}')\delta(t-t')$, m_1 and $m_0=2m_1$ are the atomic and molecular masses, Δ is the detuning corresponding to the energy mismatch $2\hbar\Delta = 2E_1 - E_0$ between the free two-atom state at the dissociation threshold and the bound molecular state, and χ is the coupling responsible for coherent conversion of molecules into atom pairs, e.g., via Raman transitions or a Feshbach resonance (see Refs. [18, 21] for details).

We have ignored s-wave scattering interactions because they do not significantly affect the dynamics or the correlations for durations resulting in less than $\sim 10\%$ conversion [18]. The characteristic timescale for this can be estimated using a Fermi's golden rule calculation [22], giving $t \lesssim 0.1\Gamma^{-1}$, where $\Gamma = \chi^2(m_1/2\hbar)^{3/2}\sqrt{|\Delta|}/\pi$ is the molecular decay rate. The duration of dissociation should also be shorter than the timescale for losses due to inelastic collisions [23].

We assume that the molecular BEC is initially in a coherent state, whereas the atoms are in the vacuum state. Once the dissociation is suddenly switched on [24], the trapping potentials are simultaneously switched off, so that the evolution takes place in free space. For molecules at rest, the excess of potential energy is converted into kinetic energy, $2\hbar|\Delta| \to 2\hbar^2k^2/(2m_1)$, of dissociated atom pairs with equal but opposite momenta around $\pm\mathbf{k}_0$, where $|\mathbf{k}_0| = \sqrt{2m_1|\Delta|/\hbar}$. This is the physical origin of the expected correlations between the atoms. Ideally, in the time-of-flight expansion the momentum correlations are converted into position correlations between diametrically opposite atoms in the far field. In non-ideal cases, such as in strongly inhomogeneous systems with large momentum uncertainty, or with insufficient time for expansion, the spatial correlations may degrade.

In absorption imaging the number of photons detected by each camera pixel determines the number of atoms contained in the volume of a narrow column in the imaging laser's propagation direction, which we denote as z. Denoting the area of the camera pixel about the point $\mathbf{r}\equiv\mathbf{x}_\perp=(x,y)$ on the detection plane as $A(\mathbf{r})$, the corresponding atom number operator is given by

$$\hat{N}_\mathbf{r} = \int_{A(\mathbf{r})} d\mathbf{r}' \int dz\, \hat{n}(\mathbf{r}',z) = \int_{A(\mathbf{r})} d\mathbf{r}'\, \hat{n}_\perp(\mathbf{r}'). \tag{2}$$

On a computational grid, the number operator $\hat{N}_\mathbf{r}$ is related to the integrated 2D column density $\hat{n}_\perp(\mathbf{r}) = \int dz\,\hat{n}(\mathbf{x})$ via $\hat{N}_\mathbf{r} = \hat{n}_\perp(\mathbf{r})\Delta x\Delta y$, where $\hat{n}(\mathbf{x}) = \hat{\Psi}_1^\dagger(\mathbf{x})\hat{\Psi}_1(\mathbf{x})$ is the 3D density, Δx and Δy are the lattice spacings, and $A(\mathbf{r})=\Delta x\Delta y$.

Correlation between the atom number fluctuations in a pair of different pixels can be quantified via the normalized number-difference variance ($\mathbf{r}\neq\mathbf{r}'$)

$$V_{\mathbf{r},\mathbf{r}'} = \frac{\langle[\Delta(\hat{N}_\mathbf{r}-\hat{N}_{\mathbf{r}'})]^2\rangle}{\langle\hat{N}_\mathbf{r}\rangle+\langle\hat{N}_{\mathbf{r}'}\rangle} = 1 + \frac{\langle:[\Delta(\hat{N}_\mathbf{r}-\hat{N}_{\mathbf{r}'})]^2:\rangle}{\langle\hat{N}_\mathbf{r}\rangle+\langle\hat{N}_{\mathbf{r}'}\rangle}, \tag{3}$$

where $\Delta\hat{C} = \hat{C} - \langle\hat{C}\rangle$ is the fluctuation in $\hat{C}$ and the colons :: indicate normally-ordered operator products. This definition uses the conventional normalization with respect to the shot-noise level of Poissonian statistics, such as for a coherent state, $\langle\hat{N}_\mathbf{r}\rangle+\langle\hat{N}_{\mathbf{r}'}\rangle$. $V_{\mathbf{r},\mathbf{r}'}=1$ for uncorrelated signals. Variance smaller than one, $V_{\mathbf{r},\mathbf{r}'}<1$, implies reduction (or squeezing) of fluctuations below the shot-noise level and is due to correlation between particle number fluctuations in the $\mathbf{r}$ and $\mathbf{r}'$ pixels. Perfect (100%) squeezing of the number-difference fluctuations corresponds to $V_{\mathbf{r},\mathbf{r}'}=0$.

The number-difference variance is related to Glauber's second-order correlation function $g^{(2)}(\mathbf{r},\mathbf{r}') = \langle:\hat{n}_\perp(\mathbf{r})\hat{n}_\perp(\mathbf{r}'):\rangle/(\langle\hat{n}_\perp(\mathbf{r})\rangle\langle\hat{n}_\perp(\mathbf{r}')\rangle)$. In the simplest symmetric case, with $\langle\hat{n}_\perp(\mathbf{r})\rangle = \langle\hat{n}_\perp(\mathbf{r}')\rangle$ and $g^{(2)}(\mathbf{r},\mathbf{r}) = g^{(2)}(\mathbf{r}',\mathbf{r}')$, the relationship is

$$V_{\mathbf{r},\mathbf{r}'} = 1 + \langle\hat{N}_\mathbf{r}\rangle[g^{(2)}(\mathbf{r},\mathbf{r}) - g^{(2)}(\mathbf{r},\mathbf{r}')]. \tag{4}$$

In order that $V_{\mathbf{r},\mathbf{r}'}$ is suppressed below the level of classical, uncorrelated statistics, $V_{\mathbf{r},\mathbf{r}'}<1$, it is necessary and sufficient to have $g^{(2)}(\mathbf{r},\mathbf{r}') > g^{(2)}(\mathbf{r},\mathbf{r})$ which is a direct signature of the violation of the classical Cauchy-Schwartz inequality [25]. Similarly, $V_{\mathbf{r},\mathbf{r}'}\geq 1$, implies $g^{(2)}(\mathbf{r},\mathbf{r}') \leq g^{(2)}(\mathbf{r},\mathbf{r})$ which agrees with the classical Cauchy-Schwartz inequality. Thus, Eq. (4) shows that to have a non-trivial quantum correlation it is not enough to have $g^{(2)}(\mathbf{r},\mathbf{r}')>1$, but one has to have $g^{(2)}(\mathbf{r},\mathbf{r}') > g^{(2)}(\mathbf{r},\mathbf{r})$. Note that a non-ideal atom detection efficiency adds a factor of $\eta<1$ to the second term in Eq. (4), but does not affect the Cauchy-Schwartz inequality.

An immediate consequence of Eq. (4) is that the observed number-difference squeezing can be insignificant if the pixel occupation number $\hat{N}_\mathbf{r}$ is very small due to a small pixel size, even if the pair correlation $g^{(2)}(\mathbf{r},\mathbf{r}')$ is much larger than $g^{(2)}(\mathbf{r},\mathbf{r})$. In other words, fine spatial resolution can degrade the number-difference squeezing between the elementary pixels, and larger pixel size or binning favor observing strong squeezing.

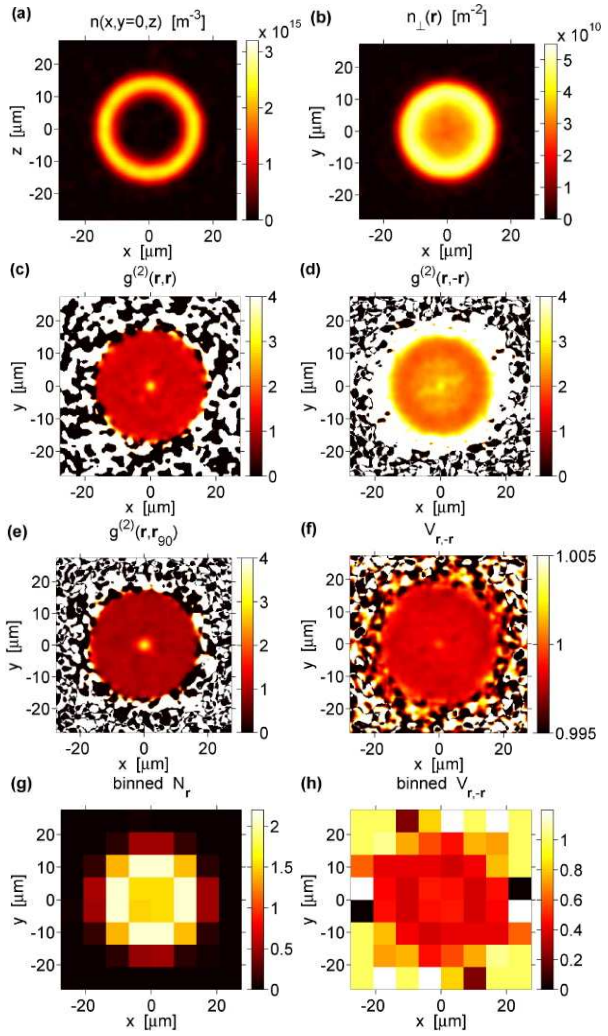

FIG. 1: (color online) Dissociation of a molecular condensate in free space, for dissociation time of $t = 0.2$ ms with $\chi = 7 \times 10^{-7}$ m$^{3/2}$ s^{-1} and a further expansion of $t_e = 2.5$ ms with $\chi = 0$ [26]. Each dimension is 55 μm long and contains 256 lattice points. 10,000 stochastic paths were averaged. (a) Slice through $z = 0$ of the 3D atomic density $n(\mathbf{x}) = \langle \hat{n}(\mathbf{x}) \rangle$ after expansion. (b) 2D column density $n_\perp(\mathbf{r}) = \langle \hat{n}_\perp(\mathbf{r}) \rangle$ after integration along the z axis. (c) local pair-correlation, $g^{(2)}(\mathbf{r}, \mathbf{r})$. The $g^{(2)}$ data is too noisy outside the dissociation sphere where the signal is negligible and should be discarded at radii $r \gtrsim 15$ μm. (d) Pair-correlation at opposite locations, $g^{(2)}(\mathbf{r}, -\mathbf{r})$. (e) Pair-correlation $g^{(2)}(\mathbf{r}, \mathbf{r}_{90})$ at orthogonal locations. (f) Number-difference variance $V_{\mathbf{r},-\mathbf{r}}$ at opposite locations. (g) Binned atomic signal on the detection plane, for bins of size 32×32 pixels, and (h) number-difference variance between the opposite bins.

Fig. 1 shows the results of a simulation of the dissociation of a small molecular BEC of size ~ 1.4 μm, containing about 205 molecules (in subsequent examples we simulate larger condensates, containing 874 and 9.2×10^3 molecules [26]). The images relate to the atomic field after dissociation and expansion. There are about 30 atoms in total in this example, corresponding to 7% conversion.

Fig. 1(a) shows a slice through the 3D atomic density, which forms an expanding spherical shell about 14 μm in radius. Fig. 1(b) shows the 2D column density after integration along the z axis. The projection of the spherical shell of atoms is clear and is similar to the experimental observations of Refs. [10, 13]. Figs. 1(c)-(d) show correlations in column densities at the same, opposite, and orthogonal locations: (c) shows the local pair correlation, $g^{(2)}(\mathbf{r}, \mathbf{r})$, which has a thermally bunched character in 3D, $g^{(2)}(\mathbf{x}, \mathbf{x}) = 2$ [18], while the obtained value of $g^{(2)}(\mathbf{r}, \mathbf{r}) \simeq 1.2 < 2$ is due to the integration along z; (d) shows strong pair-correlation at opposite locations, $g^{(2)}(\mathbf{r}, -\mathbf{r}) \simeq 2.05 > g^{(2)}(\mathbf{r}, \mathbf{r})$, originating from the momentum correlations of dissociated atom pairs; and (e) shows an uncorrelated signal of $g^{(2)}(\mathbf{r}, \mathbf{r}_{90}) \simeq 1$, where $\mathbf{r}_{90}$ corresponds to a 90° rotation of the original image about the origin. In (a)-(f), the elementary pixel size is given by the computational grid, with 0.215 μm spacing in each dimension. The numerical convergence of our simulations is ensured by smaller grid sizes reproducing the results within the stochastic sampling errors.

In the example of Fig. 1 we have a violation of the classical Cauchy-Schwartz inequality as $g^{(2)}(\mathbf{r}, -\mathbf{r}) > g^{(2)}(\mathbf{r}, \mathbf{r})$. However, due to small occupation numbers of the elementary pixels, $\langle \hat{N}_\mathbf{r} \rangle$, the associated number-difference variance at the diametrally opposite locations, $V_{\mathbf{r},-\mathbf{r}}$, shows very little squeezing in Fig. 1(f), as explained by Eq. (4); it deviates from $V_{\mathbf{r},-\mathbf{r}} = 1$ by only -1.7×10^{-3} on the projected dissociation sphere where the signal is maximal. Figs. 1(g) and (h) show that measurement bins of size 32×32 pixels improve the number difference squeezing to $V_{\mathbf{r},-\mathbf{r}} \simeq 0.4$ (60% squeezing).

To understand the dependence of the correlation strength on the initial size of the molecular BEC and the expansion time, we analyzed the binned number-difference variance for three different cases. Fig. 2 shows the dependence of the angle averaged variance $\overline{V}_{\mathbf{r_0},-\mathbf{r_0}}$ on the expansion time, for different bin sizes. At each time, the angle averaged result is at the radius r_0 of the dissociation sphere, where the signal is maximal.

As we see from Fig. 2, the squeezing improves with larger bin sizes in all cases, consistent with the experimental results of Ref. [13]. For the case of a small condensate, Fig. 2(a), the squeezing degrades with the expansion time due to the large momentum uncertainty of the initial molecular BEC. The resulting center-of-mass momentum offset of correlated atom pairs, causes them to fail to appear in diametrically opposite bins in the far field. Increasing the bin size captures the pairs in the opposite (larger) bins and restores the pair correlations. For a larger molecular condensate, as in Fig. 2(c), the complimentary effect is that the position uncertainty may give the atom pairs a center-of-mass position offset, again preventing them from appearing in the diametrically opposite bins in the near field. In this case, the squeezing improves with expansion, corresponding to a more

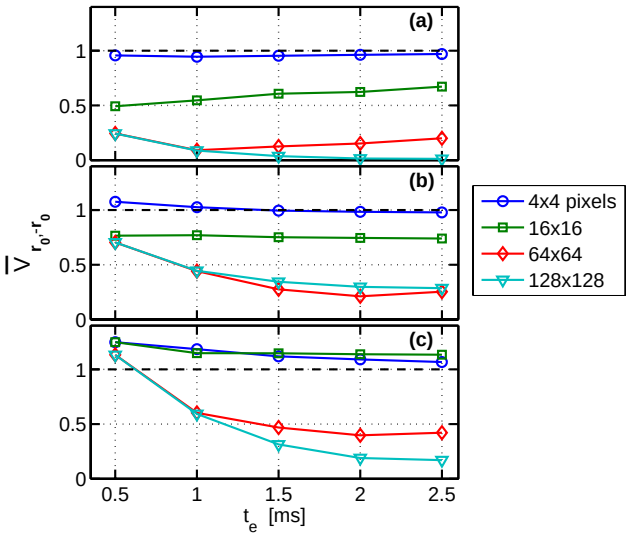

FIG. 2: (color online) The effect of binning on the angle averaged number-difference variance between the opposite bins, $\overline{V}_{\mathbf{r_0},-\mathbf{r_0}}$, as a function of the expansion time t_e following 0.2 ms of dissociation. Graphs (a), (b) and (c) correspond, respectively, to the initial molecular BEC size of 1.4, 3 and 6.4 μm [26]. The different curves are for different bin sizes. The largest bins into just four quadrants on the detection plane.

complete conversion of the intrinsic opposite-momentum correlations into spatial correlations in the far field. The case of Fig. 2(b) is intermediate and is affected by the competition between these two effects, resulting in the optimum expansion time and implying the existence of an optimum size of the molecular BEC for a given expansion time.

The authors acknowledge stimulating discussions with A. Perrin and C. Westbrook, and thank the developers of the XMDS software (see www.xmds.org). The work was supported by the Australian Research Council.

[1] A. Einstein, B. Podolsky, and N. Rosen, Phys. Rev. **47**, 777 (1935); N. Bohr, Phys. Rev. **48**, 696 (1935).
[2] Z. Y. Ou *et al.*, Phys. Rev. Lett. **68**, 3663 (1992).
[3] E. S. Polzik, Phys. Rev. A **59**, 4202 (1999); S. A. Haine and J. J. Hope, Phys. Rev. A **72**, 033601 (2005).
[4] H. Pu and P. Meystre, Phys. Rev. Lett. **85**, 3987 (2000); L. M. Duan *et al.*, Phys. Rev. Lett. **85**, 3991 (2000).
[5] R. Bach *et al.*, Phys. Rev. A **65**, 063605 (2002); V. A. Yurovsky, Phys. Rev. A **65**, 033605 (2002); A. A. Norrie *et al.*, Phys. Rev. Lett. **94**, 040401 (2005); P. Deuar and P. D. Drummond, Phys. Rev. Lett. **98**, 120402 (2007).
[6] T. Opatrný and G. Kurizki, Phys. Rev. Lett. **86**, 3180 (2001); U. V. Poulsen and K. Mølmer, Phys. Rev. A **63**, 023604 (2001).
[7] K. V. Kheruntsyan and P. D. Drummond, Phys. Rev. A **66**, 031602 (2002); K. V. Kheruntsyan, Phys. Rev. A **71**, 053609 (2005).
[8] V. A. Yurovsky and A. Ben-Reuven, Phys. Rev. A **67**, 043611 (2003).
[9] K. V. Kheruntsyan, M. K. Olsen, and P. D. Drummond, Phys. Rev. Lett. **95**, 150405 (2005).
[10] S. Dürr, T. Volz, and G. Rempe, Phys. Rev. A **70**, 031601(R) (2004).
[11] M. W. Jack and H. Pu, Phys. Rev. A **72**, 063625 (2005).
[12] K.V. Kheruntsyan, Phys. Rev. Lett. **96**, 110401 (2006).
[13] M. Greiner *et al.*, Phys. Rev. Lett. **94**, 110401 (2005).
[14] A. Perrin *et al.*, arXiv: 0704.3047v1; A. Perrin, C. M. Savage, V. Krachmalnicoff, D. Boiron, C. I. Westbrook, and K. V. Kheruntsyan (to be published).
[15] E. Altman, E. Demler, and M. D. Lukin, Phys. Rev. A **70**, 013603 (2004).
[16] S. Fölling *et al.*, Nature (London) **434**, 481 (2005).
[17] M. Yasuda and F. Shimizu, Phys. Rev. Lett. **77**, 3090 (1996); M. Schellekens *et al.*, Science **310**, 648 (2005).
[18] C. M. Savage, P. E. Schwenn, and K. V. Kheruntsyan, Phys. Rev. A **74**, 033620 (2006).
[19] The role of confinement in dissociation has been studied by: I. Tikhonenkov and A. Vardi, Phys. Rev. Lett. **98**, 080403 (2007).
[20] P. D. Drummond and C. W. Gardiner, J. Phys. A **13**, 2353 (1980).
[21] D. J. Heinzen *et al.*, Phys. Rev. Lett. **84**, 5029 (2000); P. D. Drummond and K. V. Kheruntsyan, Phys. Rev. A **70**, 033609 (2004).
[22] M. J. Davis, S. J. Thwaite, M. K. Olsen, and K. V. Kheruntsyan, arXiv:0710.4257.
[23] N. Syassen *et al.*, Phys. Rev. A **74**, 062706 (2006).
[24] T. M. Hanna *et al.*, Phys. Rev. A **74**, 023618 (2006).
[25] M.D. Reid and D.F. Walls, Phys. Rev. A **34**, 1260 (1986).
[26] Fig. 1 is for the initial molecular BEC in a spherically symmetric harmonic trap of frequency $\omega/2\pi = 90$ Hz, with a density profile given by the ground-state of the Gross-Pitaevskii equation, obtained for $^{87}Rb_2$ dimers at a scattering length of 2 nm, as an example. The chemical potential is chosen to give a peak density of 5×10^{19} m^{-3}, which results in a total of 205 molecules and a half-width of ~ 1.4 μm. In the two additional examples of Fig. 2, the trap frequencies are $\omega/2\pi = 45$ Hz and 19 Hz, while the chemical potentials are adjusted to result in the same peak density, giving a total of 874 and 9.2×10^3 molecules, respectively, and half-widths of ~ 3 μm and ~ 6.4 μm. The detuning is $\Delta/2\pi = -3$ kHz in all cases.